Lattice Boltzmann Study of the Water Droplet on a Surface Corrugated with Nanopillars#

Jihye Jang, Sung Woo Park, Hyojeong Kim, Mohammad A. Matin, Zhengqing Zhang, and Joonkyung Jang*

*Department of Nanomaterials Engineering and BK21 Plus Nano Convergence Technology Division, Pusan National University, Busan 609-735, Republic of Korea. *E-mail: jkjang@pusan.ac.kr*
Received October 31, 2014, Accepted November 19, 2014, Published online February 26, 2015

Using the lattice Boltzmann method, we simulated a water droplet on a surface covered with rectangular or parabolic pillars. With increasing spacing between the pillars, the transition from the Cassie to Wenzel states of the droplet was observed. The critical spacing at which the transition occurs and the contact angle of droplet were compared with those obtained from the macroscopic theories of Cassie and Wenzel. The present simulation revealed intermediate states where the droplet was partially impaled by the pillars. Even in the Cassie state, the droplet significantly penetrated down in the gap between the parabolic pillars.

Keywords: Lattice Boltzmann method, Wenzel, Cassie, Superhydrophobic surface, Contact angle

Introduction

Corrugating a surface with small pillars can greatly enhance the hydrophobicity of a surface. Lotus leaves, for example, have numerous parabolic pillars on their surfaces, so that the water droplets have high contact angles (>120°) and are very mobile on these leaves.[1] Micro- and nano-pillars of various shapes have been constructed to produce superhydrophobic surfaces. Typically, parabolic or rectangular pillars are periodically constructed and the spacing between pillars is systematically varied to achieve the highest contact angle of a water droplet on such a pillared surface.

The contact angle and mobility of a water droplet on a pillared surface critically depends on whether the droplet is impaled by the pillars or not (see Figure 1). The former and latter cases are, respectively, called the Wenzel and Cassie states of the droplet. The contact angle of a droplet in the Wenzel state θ^{WZ} is given by[2]

$$\cos\theta^{WZ} = r^{WZ}\cos\theta_i \quad (1)$$

where θ_i is the *intrinsic* contact angle of a macroscopic droplet deposited on a *flat* surface and r^{WZ} (>1) is the ratio of the total solid surface area to the projected area in the horizontal plane. On the other hand, the contact angle of a droplet in the Cassie state θ^{CB} is[3]

$$\cos\theta^{CB} = f^{CB}(1+\cos\theta_i) - 1 \quad (2)$$

where f^{CB} (<1) is the fraction of the solid surface area in contact with the droplet to the solid surface area projected onto the horizontal plane. In both the Wenzel and Cassie theories above, the droplet is assumed to be infinitely large relative to the size of pillar.

Note that the gap between the pillars is empty for the Cassie state but filled with liquid for the Wenzel state. Microscopically, the Wenzel or Cassie state of a droplet should be determined by the interplay between the intermolecular cohesion and interfacial energy of the water confined in the gap between the pillar walls. With decreasing inter-pillar spacing S, the water confined between the pillars reduces its volume and its degree of cohesion. Below a critical value S_C, the confined liquid is unstable and evaporates, giving rise to a Cassie state.

In designing a hydrophobic pillared surface, one would like to know how the Cassie or Wenzel state of the droplet is

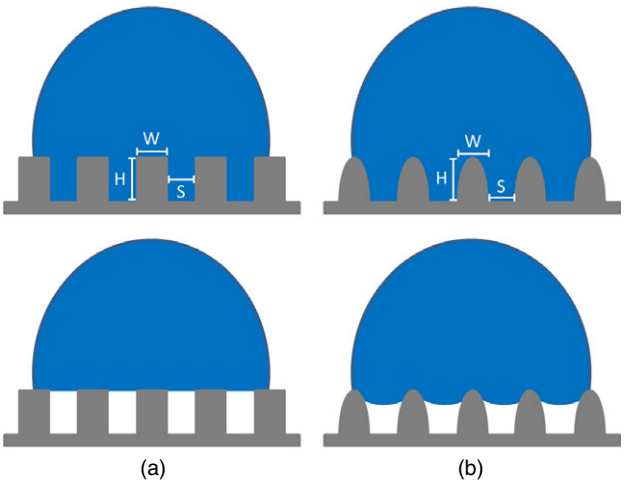

Figure 1. Schematic illustration of the Wenzel (top) and Cassie (bottom) states of a water droplet resting on the periodic array of rectangular (a) or parabolic (b) pillars. *W* and *H* refer to the width and height of each pillar, respectively, and the spacing between neighboring pillars is denoted by *S*.

This paper is dedicated to Professor Kwan Kim on the occasion of his honorable retirement.

affected by the spacing between pillars. Exploring this experimentally is costly and time consuming. Theoretical investigation therefore emerges as a viable option for this quest. Here we employ the lattice Boltzmann method (LBM) to study this aspect. The LBM is a microscopic and dynamic approach that enables us to study the structure and dynamics of the water droplet,[4–10] which is not available in the macroscopic Cassie and Wenzel theories. Specifically, we examine the transition between the Wenzel and Cassie states by systematically varying the inter-pillar spacing S for a periodic array of rectangular or parabolic pillars. We calculate the critical spacing at which Cassie-to-Wenzel transition occurs and the contact angles of the water droplets on these pillared surfaces. These results are compared with the Wenzel and Cassie theories. We also investigate the dynamics of a water droplet that was initially in the Wenzel state and eventually in the Cassie state.

Simulation Method

We simulated a two-dimensional (2D) periodic array of rectangular or parabolic pillars on a flat surface (see Figure 1). The width W and height H of pillar and the spacing between pillars S are defined in Figure 1. Both W and H were set to 21 grid spacings.

In the LBM simulation, the time evolution of the distribution function $f_i(x, t)$ was numerically solved on a 2D square grid, D2Q9. At each grid point x, nine discrete velocity vectors e_is (i = 0–8) are assigned (four for horizontal moves, four for diagonal moves, and one for no move). The effects of streaming and collision on each grid point are considered as[11]

$$f_i(x+e_i\Delta t, t+\Delta t) = f_i(x,t) - \frac{[f_i(x,t) - f_i^{eq}(x,t)]}{\tau} \quad (3)$$

where τ is the relaxation time for equilibration, and Δt is the time step. τ is related to fluid kinematic viscosity ν as $\nu = 1/3(\tau - 1/2)$.[4] Choosing $\tau = 0.7$ gave an intrinsic contact angle typical for a hydrophobic surface. The equilibrium distribution function $f_i^{eq}(x,t)$ is given by

$$f_i^{eq}(x,t) = \omega_i \rho(x,t)\left[1 + 3\frac{e_i\cdot u}{c^2} + \frac{9}{2}\frac{(e_i\cdot u)^2}{c^4} - \frac{3}{2}\frac{u^2}{c^2}\right] \quad (4)$$

where the weight factors ω_is are 1/9 for vertical and horizontal moves, 1/36 for diagonal movements, and 4/9 for no movement. c is the grid spacing per time step. The attraction between nearest neighbor fluid particles is modeled by using the method of Shan and Chen.[12] The fluid–solid interaction was taken into account by following Martys and Chen.[13] All quantities are reported in the units of grid spacing and time step Δt.

A square grid with a size of 461 × 250 points was used. In the case of a flat surface, a water droplet rectangular in shape (301 × 151) was initially placed on the surface. For a pillared surface, a rectangular water droplet was initially placed on top of the pillars and the gap between pillars was filled with the droplet (Wenzel state). The inter-pillar spacing S was varied as 3, 5, 10, 15, and 20.

We calculated the contact angle of a droplet from the scaled density ρ_S of each grid point, which is defined as the density divided by the highest density. The contour line of $\rho_S = 0.5$ (Figure 2) was taken to be the periphery of the droplet (drawn as circles in Figure 2). The periphery points were then fitted to a quadratic function, $y = Ax^2 + Bx + C$. The resulting fit is drawn as the red line in Figure 2. The contact angle was obtained from the tangential line at $y = 0$ (broken line in Figure 2).[14] We simulated droplets with various sizes whose base radii R_Bs varied as 81, 97, 132, and 149. The corresponding contact angles θs decreased with increasing the size of droplet as 110.53°, 109.07°, 107.47°, and 108.86°. The modified Young's equation predicts $\cos\theta$ is a linear function of $1/R_B$ given by[15]

$$\cos\theta = \cos\theta_i - \gamma_{slv}/(R_B\gamma_{lv}) \quad (5)$$

where γ_{slv} is the solid–liquid–vapor line tension and γ_{lv} is the liquid–vapor surface tension. By fitting the four values of $\cos\theta$ to a linear function of $1/R_B$, the intrinsic contact angle was estimated from the fit value at $1/R_B = 0$. The resulting θ_i was 98.94°.

The Wenzel and Cassie theories, Eqs. (1) and (2) were implemented by calculating r^{WZ} and f^{CB} as follows. r^{WZ}s for the surfaces covered with the rectangular and parabolic pillars are, respectively, given by $1 + 2H/(W + S)$ and $(p/2)/(W + S)$. Here, p is an approximate circumference of the parabola given by $\pi\left[(W/2+H) - \sqrt{(3W/2+H)(W/2+3H)}\right]$.[16] f^{CB} of the surface covered with the rectangular pillars is given by $W/(W + S)$. f^{CB} for a surface covered with the parabolic pillars is 0 if the droplet does not penetrate down into the gap between the pillars. In the LBM simulation, however, the droplet partially penetrated down into the gap. We therefore calculated f^{CB} from the LBM simulation by measuring the projected area of the parabolic surface in contact with the droplet.

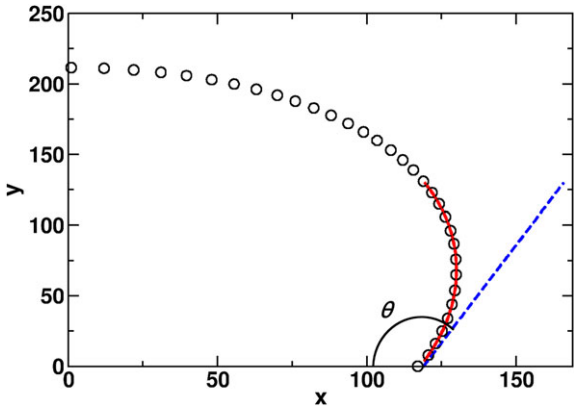

Figure 2. Periphery of a water droplet on a flat surface. Drawn as circles are the peripheral points obtained from the present LBM simulation ($\rho_s = 0.5$). The red line is the quadratic fit to the peripheral points. The broken line represents the tangential line at $y = 0$, which is used to calculate the contact angle θ.

Results and Discussion

Shown in Figure 3 are the equilibrium snapshots of the water droplets deposited on rectangular (left) and parabolic (right) pillars. These snapshots were taken at the time of 30 000. Typically, the equilibrium was reached within 3000 time steps. As S increased from 3 (top) to 5, 10, 15, and 20, the water droplet in the Cassie state penetrated down into the inter-pillar gap to be in the Wenzel state. Notice that the Cassie-to-Wenzel transition at $S = 5$ (second from top) is incomplete, however. Only a portion of the inter-pillar gap below the droplet is filled with the droplet and the rest of the gaps are empty. These intermediate states persisted even after running the simulation for 40 000 time steps.

In case of a macroscopic droplet, the state with a lower contact angle is thermodynamically stable.[17] In this perspective, the transition between the Cassie and Wenzel states occurs when the contact angles from the Cassie (Eq. (2)) and Wenzel (Eq. (1)) theories become identical. The S_C obtained this way is drawn as a vertical line in Figure 4. We also show the S_C from simulation, which was directly observed in the LBM simulation. One can see that the macroscopic theory slightly underestimates S_C relative to the LBM value.

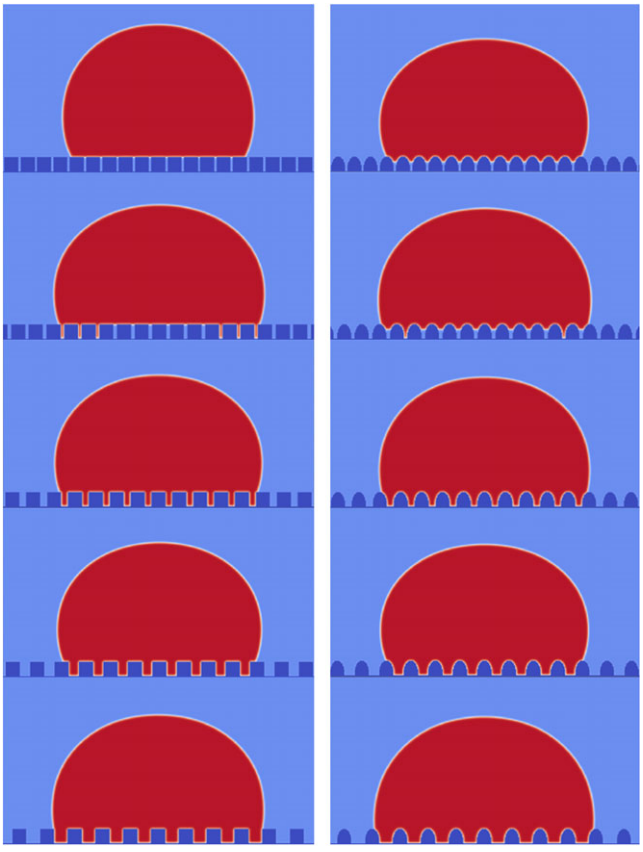

Figure 3. Cassie-to-Wenzel transition of a droplet on a surface covered with rectangular (left column) or parabolic (right column) pillars. As the inter-pillar spacing increases from 3 (top) to 5 (second from top), 10 (middle), 15 (second from bottom), and 20 (bottom), the droplet changes its state from a Cassie state (top) to a Wenzel state.

We investigated the contact angles of the water droplets in simulation and compared them with those predicted from the Wenzel and Cassie theories, Eqs. (1) and (2). In Figure 4, the contact angle is plotted versus S for the surfaces covered with the rectangular (a) and parabolic (b) pillars. Overall, the LBM contact angle decreased with increasing inter-pillar spacing, ranging from 112.6° to 100.2°. One can see, however, that the contact angle slightly increases by increasing S from 10 to 15. This contrasts with the monotonic decrease of the Wenzel contact angle (solid line) with increasing S. Overall, both the Wenzel (solid line) and Cassie (dotted line) theories are in agreement with the LBM simulation. The Wenzel theory contact angles are consistent with the overall decreasing feature of the LBM simulation results.

We studied the dynamics of the transition from the Wenzel to Cassie state. Shown in Figure 5 are the time evolutions of the droplets initially filling the gap between rectangular (a) and parabolic (b) pillars ($S = 5$). The bottom surface of the droplet

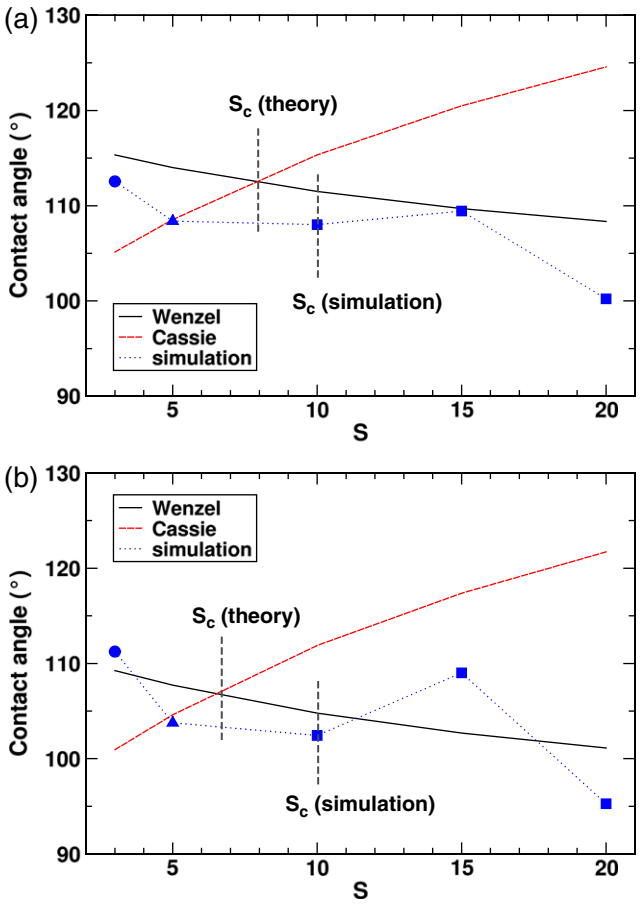

Figure 4. Contact angle of the water droplet resting on an array of rectangular (a) or parabolic (b) pillars. The contact angle is plotted versus the inter-pillar spacing S. The circles, triangles, and squares, respectively, represent the Cassie, intermediate, and Wenzel states. The lines connecting symbols are drawn for visual guidance. The contact angles from the Wenzel and Cassie theories are plotted as solid and dotted lines, respectively. Drawn as the vertical lines are the critical inter-pillar spacing at which the Cassie-to-Wenzel transition occurs S_c.

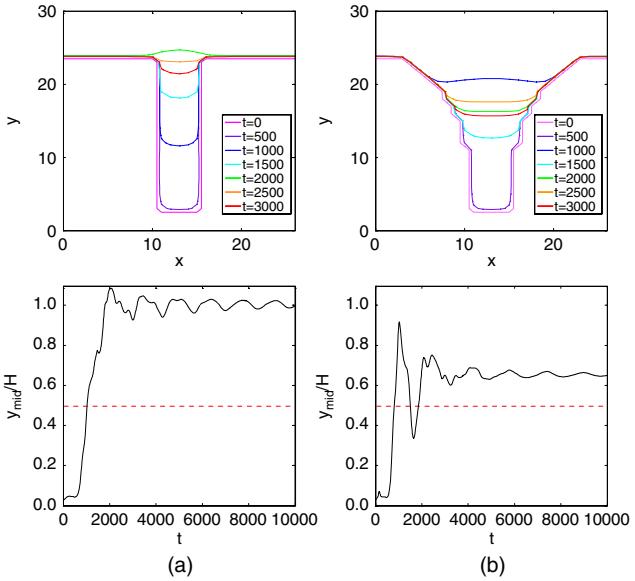

Figure 5. Time evolution of the Wenzel to Cassie state of the water droplet initially filling the gap between the rectangular (a) or parabolic (b) pillars. At the top, the bottom surface of the water droplet is drawn for different times. At the bottom, we plot the time variation of the height of the droplet in the middle of the pillar walls y_{mid}. We plot y_{mid} scaled by the height of pillar H. Drawn as horizontal dotted lines are the positions of the half heights of the pillars.

eventually moved up to the top of the pillars (see the top two panels). The surface of the droplet temporarily moved up and down. This can be clearly seen in the time-dependent y position of the bottom of the droplet at the midpoint between the pillar walls, y_{mid} (bottom two panels of Figure 5). The time oscillation in y_{mid} is evident, especially for the gap between parabolic pillars. y_{mid} was near the bottom of the pillar ($y = 0$) for short times, but it abruptly rose to the top of the pillar starting at times 491 and 474 for rectangular and parabolic pillars, respectively. y_{mid} for the gap between the rectangular pillars stayed near the top of the pillars ($y_{mid}/H = 1$) but it converged to 0.65 for the parabolic pillars. Therefore, one can see the droplet in the Cassie state significantly penetrates down into the gap between the parabolic pillars. In the top two panels of Figure 5, one can also observe that the curvature of the liquid surface can be upward at times ($t = 2000$ for the rectangular pillars and $t = 1000$ for the parabolic pillars). This type of inversion of the curvature occurs when a liquid surface touches the corner where two solid planes cross each other.[18]

Although we tried to mimic the parabolic shapes of pillars on the lotus leaves, real lotus leaves have a hierarchical structure where microscale pillars are topped with nanoscale pillars. The present study only considered the primary shapes of the pillars found on lotus leaves. Besides, only 2D pillars were considered because of computational simplicity. In the future, we hope to model realistically the 3D and hierarchical nature of the pillars on lotus leaves.

Conclusion

The surfaces corrugated with periodic pillars are widely utilized as superhydrophobic surfaces. It is therefore important to understand how the hydrophobicity of such a pillared surface is affected by the shape of pillar and the spacing between pillars. By employing the microscopic LBM simulation, we studied the water droplet on an array of rectangular or parabolic pillars. By varying the spacing between neighboring pillars, we examined whether the droplet is impaled by pillars (Cassie state) or not (Wenzel state). Compared to the LBM simulation, the macroscopic Cassie and Wenzel theories underestimated the inter-pillar spacing at which the Cassie-to-Wenzel transition occurs. Overall, the contact angle of the water droplet from the Cassie or Wenzel theory was in agreement with that of the LBM simulation. Interestingly, we found states intermediate between the Wenzel and Cassie states where the water droplet is partially impaled. The Cassie droplet on the parabolic pillars significantly penetrated down in the gap between pillars.

Acknowledgment. This work was supported by the Convergence Research Grant funded by the Pusan National University (PNU, Convergence Research Grant) (PNU-2013-000-201313110001).

References

1. V. Zorba, E. Stratakis, M. Barberoglou, E. Spanakis, P. Tzanetakis, S. H. Anastasiadis, C. Fotakis, *Adv. Mater.* **2008**, *20*, 4049.
2. R. N. Wenzel, *Ind. Eng. Chem.* **1936**, *28*, 988.
3. A. B. D. Cassie, S. Baxter, *Trans. Faraday Soc.* **1944**, *40*, 546.
4. M. Gross, F. Varnik, D. Raabe, I. Steinbach, *Phys. Rev. E* **2010**, *81*, 051606.
5. R. J. Vrancken, H. Kusumaatmaja, K. Hermans, A. M. Prenen, O. Pierre-Louis, C. W. M. Bastiaansen, D. J. Broer, *Langmuir* **2009**, *26*, 3335.
6. M. Sbragaglia, A. M. Peters, C. Pirat, B. M. Borkent, R. G. H. Lammertink, M. Wessling, D. Lohse, *Phys. Rev. Lett.* **2007**, *99*, 156001.
7. B. Zhang, J. Wang, X. Zhang, *Langmuir* **2013**, *29*, 6652.
8. H. Kusumaatmaja, J. M. Yeomans, *Langmuir* **2007**, *23*, 6019.
9. H. Kusumaatmaja, R. J. Vrancken, C. W. M. Bastiaansen, J. M. Yeomans, *Langmuir* **2008**, *24*, 7299.
10. Y. Kim, W. Choi, J. Lee, *Microfluid. Nanofluid.* **2011**, *10*, 173.
11. P. L. Bhatnagar, E. P. Gross, M. Krook, *Phys. Rev.* **1954**, *94*, 511.
12. X. Shan, H. Chen, *Phys. Rev. E* **1994**, *49*, 2941.
13. N. S. Martys, H. Chen, *Phys. Rev. E* **1996**, *53*, 743.
14. N. Giovambattista, P. G. Debenedetti, P. J. Rossky, *J. Phys. Chem. B* **2007**, *111*, 9581.
15. J. Y. Wang, S. Betelu, B. M. Law, *Phys. Rev. E* **2001**, *63*, 031601.
16. S. Ramanujan, *Quart. J. Pure Appl. Math.* **1914**, *45*, 350.
17. A. Marmur, *Langmuir* **2003**, *19*, 8343.
18. A. Giacomello, M. Chinappi, S. Meloni, C. M. Casciola, *Phys. Rev. Lett.* **2012**, *109*, 226102.

